Atmospheric Environment 240 (2020) 117830

Contents lists available at ScienceDirect

Atmospheric Environment

journal homepage: http://www.elsevier.com/locate/atmosenv

Long-term trends and variations in haze-related weather conditions in north China during 1980–2018 based on emission-weighted stagnation intensity

Jin Feng [a,*], Hong Liao [b], Yanjie Li [c], Ziyin Zhang [a], Yingxiao Tang [d]

[a] Institute of Urban Meteorology (IUM), China Meteorological Administration (CMA), Beijing, China
[b] Jiangsu Key Laboratory of Atmospheric Environment Monitoring and Pollution Control, Jiangsu Collaborative Innovation Center of Atmospheric Environment and Equipment Technology, School of Environmental Science and Engineering, Nanjing University of Information Science & Technology, Nanjing 210044, China
[c] State Key Laboratory of Numerical Modeling for Atmospheric Sciences and Geophysical Fluid Dynamics (LASG), Institute of Atmospheric Physics (IAP), Chinese Academy of Science (CAS), Beijing, China
[d] Tianjin Environmental Meteorological Center, Tianjin, 300074, China

HIGHLIGHTS

- New emission-weighted index to characterize the intensity of air stagnation.
- The index has a close spatial relationship with $PM_{2.5}$ observations in North China.
- The index reflects low-frequency variability in haze-related weather conditions.
- Increasing stagnation over 1980–2018, with a drop since 2013, in North China.
- Significant stagnation variability challenges the emission reduction plan.

ARTICLE INFO

Keywords:
Haze
North China
Stagnation

ABSTRACT

Recently, climatological and environmental researchers have paid significant attention to the long-term trends and variations in haze-related weather conditions in North China (NC). This study investigates this topic using a quantified air stagnation index (ASI_E) that combines stagnation intensity with fixed emission information, given that haze occurrence depends strongly on the rate of emission. ASI_E has a close spatial and temporal relationship with observed $PM_{2.5}$ concentrations, and a strong sensitivity to haze occurrence in NC. The annual ASI_E increased by 18.2% over the period 1980–2018 due to significant decreases in planetary boundary layer height and ventilation. However, there was an apparent drop during 2013–2018, which suggests that lower stagnation intensity may take effect on the improved air quality in NC reported in recent years. Such low-frequency oscillation occurred twice during 1980–2018. Hence, if the current trend of decreasing stagnation intensity reverses, haze events may become more common in the future. In addition, the interannual variations in stagnation intensity were very significant. The percentage change of ASI_E was as high as 50%–70% in some years. Finally, using the year-to-year growth ratio of ASI_E, we highlight the difficulty of the "clean air challenge" due to the variations in stagnation in NC. The results suggest that the enforcement of the emission reduction plan should be tailored according to the stagnation conditions in the region and period of interest.

1. Introduction

The increasing frequency of haze events in North China (NC) during the last decade has motivated considerable effort to understand the long-term variation in haze-related meteorological conditions. This is helpful for understanding the interannual variation (IAV) and long-term trends in NC air quality (Feng et al., 2016), given the lack of national in-situ aerosol monitoring networks before 2013 (Ma et al., 2014; Xin et al., 2016). Studies have shown that various large-scale atmospheric or oceanic circulation systems influence NC haze, such as the East Asian

* Corresponding author. Institute of Urban Meteorology (IUM), Beijing, 100089, China.
E-mail address: jfeng@ium.cn (J. Feng).

https://doi.org/10.1016/j.atmosenv.2020.117830
Received 8 January 2020; Received in revised form 27 July 2020; Accepted 29 July 2020
Available online 1 August 2020

Monsoon (Zhu et al., 2012; Yin and Wang, 2016), Arctic Oscillation (Xiao et al., 2014; Yin and Wang, 2016), East Asian Trough and East Asian Jet (Chen and Wang, 2015), Pacific Decadal Oscillation (Zhao et al., 2016) and North Atlantic Oscillation (Chen et al., 2019). Circulation indexes have also been proposed and used for haze projection (Cai et al., 2017; Pei et al., 2018).

However, circulation does not directly determine the occurrence of haze. Instead, the circulation affects local weather processes such as aerosol diffusion or wet deposition. In NC, the occurrence, development and extinction of these haze events are closely related to the variations in air stagnation intensity. Strong air stagnation is characterized by weak diffusion in the boundary layer and absence of precipitation (Wang and Angell, 1999; Feng et al., 2018; Wang et al., 2018), providing favorable meteorological conditions for rapid accumulation of severe pollution (Sun et al., 2015). When the stagnation intensity weakens, air quality tends to improve (Wang et al., 2016). Recent extreme haze events in NC, with observed maximum $PM_{2.5}$ concentrations exceeding 600 μg m^{-3}, were caused by air stagnation (Quan et al., 2014; Zhang et al., 2014; Ye et al., 2016, Shao et al., 2018a, b). Some studies have also reported that the long-term variation in aerosol concentrations in NC can be modulated by long-term variations in air stagnation (Fu et al., 2014; Shao et al., 2018a, b; Hong et al., 2019).

Unfortunately, air stagnation is not a quantity that can be obtained from conventional meteorological observation networks. It must be parameterized as an air stagnation index (ASI) using conventional meteorological variables. Previous studies have proposed several ASI schemes, based mostly on various definitions of the "air stagnation day" (ASD) meeting several thresholds. For example, the earliest and commonly used ASD from NOAA (National Oceanic and Atmospheric Administration) is defined as a day on which the daily sea level geostrophic wind speed is < 8 m s^{-1}, the daily wind speed at 500 hPa is < 13 m s^{-1}, no precipitation occurs and the temperature is inverted within the planetary boundary layer (PBL) throughout the day (Wang and Angell, 1999; Horton et al., 2014; Huang et al., 2017). However, it is reported to not be applicable for the variations in aerosol pollution in China (Cai et al., 2017; Feng et al., 2018; Wang et al., 2018). There are some ASD definitions specifically defined for China, which consider thresholds of daily maximal ventilation in the atmospheric boundary layer, real latent instability (Huang et al., 2018) or planetary boundary layer height (PBLH) (Wang et al. 2016, 2018; Hong et al., 2019). These ASIs based on ASDs are a type of "frequency index" that counts the ASD numbers in a given time period (such as one month or one year). However, a frequency index cannot represent well the continuous temporal variations in stagnation intensity from daily to interdecadal timescales.

Motivated by this, Feng et al. (2018) proposed an ASI (labeled as ASI_M hereafter; see Section 2), which can provide daily stagnation intensity values at specific locations (e.g., measurement sites or grid cells of a meteorological model). The ASI_M is well correlated to the daily and monthly variations in observed $PM_{2.5}$ concentrations at most NC grid cells, and thus can reflect the synoptic situations that drive haze variation in NC. The ASI_M can be used as a prediction tool for extreme NC haze events. For five of the most aerosol-polluted cities in NC, including Beijing, the prediction accuracy is >70%. However, Feng et al. (2018) did not analyze the long-term variations in ASI_M, which would be helpful for understanding historical haze variation over NC. Furthermore, to fully investigate the haze-related meteorological conditions in NC, emission information should be considered, because the same stagnation intensity can cause very different aerosol pollution levels under different emission conditions. The lack of emission information in ASI_M means that it cannot accurately represent the spatial pattern of air quality (Fig. 1) and the geographical distribution of its trends and variations. Previous ASIs (including these circulation indexes) have experienced problems related to this issue.

Therefore, to address these limitations, an ASI that includes both the stagnation intensity and emission information is required. This study establishes an emission-weighted stagnation intensity index (referred to as ASI_E hereafter) by combining the ASI_M with a parameterized emission factor, and analyzes its climatological distribution, long-term variations and trend in NC over 1980–2018. The rest of this paper is organized as follows: Section 2 describes the details of the ASI_E scheme, the aerosol concentrations and meteorological datasets. Section 3 contains the results, with Section 3.1 presenting the performance of ASI_E using the observed $PM_{2.5}$ concentrations from September 2013 to September 2016. In Sections 3.2 and 3.3 we show the long-term variations and trends in stagnation intensity in NC, and the effects of horizontal ventilation, PBLH and precipitation on such trends and variations. In section 3.3, we also discuss the year-to-year relationship between the stagnation intensity and emission reduction, which provides some insights into the potential results of the recent emission control strategies in different areas of NC. Section 4 draws conclusions and discusses the possible future trend of stagnation intensity.

2. Methods and data

2.1. ASI_E scheme and statistical method

The ASI_M is defined as the product of three coefficients in the form:

$$ASI_M = \lambda \cdot P_V \cdot P_D \cdot P_W, \quad (1)$$

where P_V, P_D and P_W denote the parameters of ventilation, vertical diffusion and wet deposition, respectively. λ is used to keep the ASI_M

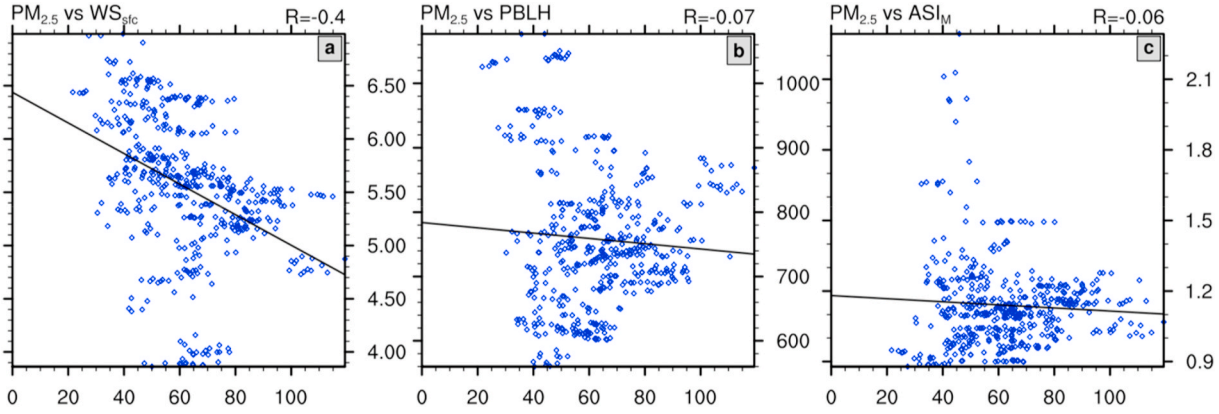

Fig. 1. Plots between time-averaged observed $PM_{2.5}$ concentrations (*x*-axis) and (a) surface wind speed (m s^{-1}), (b) PBLH (m) and (c) ASI_M (dimensionless) over NC from May 2013 to August 2016. These meteorological variables (PBLH and surface wind speed) used by ASI_M are not related to the distribution of aerosol concentrations.

dimensionless and on an order of magnitude of one. P_V is defined by a non-linear function of the height-weighted average of wind speed over the PBL as:

$$P_V = \left(\frac{1}{z_{PBL} - z_0} \int_{z_0}^{z_{PBL}} U(z)dz \right)^{-1/4}, \quad (2)$$

where $U(z)$ is the wind speed at the geopotential height z (unit: m) and z_0 and z_{PBL} are the geopotential heights of the surface and top of the PBL, respectively. P_D is simply the inverse of PBLH denoted by:

$$P_D = \frac{1}{z_{PBL} - z_0}. \quad (3)$$

P_W is designed to reflect the significant decrease (e-folding) of the stagnation conditions induced by precipitation, and is written as:

$$P_W = e^{(1-\delta(r))}, \quad (4)$$

where r is the daily mean accumulated precipitation rate (units: mm d^{-1}) and:

$$\delta(r) = \begin{cases} 1, r \geq 1, \\ 0, r < 1. \end{cases} \quad (5)$$

Finally, the ASI_M is parameterized as follows:

$$ASI_M = \frac{\lambda e^{(1-\delta(r))} \left(\frac{1}{z_{PBL} - z_0} \int_{z_0}^{z_{PBL}} U(z)dz \right)^{-1/4}}{(z_{PBL} - z_0)}, \quad (6)$$

where $\lambda = 10^3 s^{-\frac{1}{4}}$. Unlike the ASD-based indexes that are based on fixed thresholds for a series of meteorological variables, the ASI_M scheme is a parameterization of the physical processes that directly affect aerosol accumulation or elimination. The ASI_M directly represents stagnation intensity as a function of wind speed, PBLH and precipitation. It can be easily calculated according to the spatial and temporal resolution of the wind, PBLH and precipitation datasets. Its applicability to variations in $PM_{2.5}$ concentrations and haze prediction over the whole of NC has been presented in Feng et al. (2018).

To include emission information in the ASI, we propose the ASI_E scheme defined as:

$$ASI_E(x, y, t) = ASI_M(x, y, t) \cdot P_E(x, y). \quad (7)$$

Here, P_E denotes the emission factor as a spatially varying background, which can be obtained from the following three steps. First, we define the $PM_{2.5}$-related emissions (labeled as E) according to the main components of $PM_{2.5}$ and the conversion process from various precursors in the form of:

$$E = 0.22E_{[SO_2]} + 0.1E_{[NO_x]} + E_{[BC]} + 2.1E_{[OC]} + 0.17E_{[terpenes]} + E_{[OP]}, \quad (8)$$

where $E_{[SO_2]}$, $E_{[NO_x]}$, $E_{[BC]}$, $E_{[OC]}$, $E_{[terpenes]}$ and $E_{[OP]}$ are the emission quantities of SO_2, NO_x, black carbon (BC), organic carbon (OC), terpenes and other particle sources of $PM_{2.5}$, respectively (the derivation of E is set out in the supplementary material).

Second, considering that pollution at a specific location is affected by nearby emission sources, we use a smoothed emission (E_S) to represent an exponentially reduced influence of nearby emissions with distance following Lu et al. (2015) and Shao et al., 2018a, b. In addition, we consider the effects of short-range transport processes due to the prevailing wind field on emissions. The E_S at a specific grid cell (x, y) is designed to be the sum of nearby emissions weighted by distance and climatological wind fields, which is in the form of:

$$E_S(x, y) = \sum_{D_{(i,j)}(x,y) \leq D_{T_{(i,j)}}(x,y)} E_{(i,j)} \cdot \exp\left[- \frac{D^2_{(i,j)}(x, y)}{2\left(\frac{D_{T_{(i,j)}}(x,y)}{3}\right)^2} \right], \quad (9)$$

where

$$D_{T_{(i,j)}}(x, y) = D_{T0}\left[\frac{1}{2}U_{L_{(i,j)}} \cos\theta_{(i,j)}(x, y) + 1\right]. \quad (10)$$

$E_{(i,j)}$ is the $PM_{2.5}$-related emission at the grid cell (i, j) obtained from eq. (8). $D_{(i,j)}(x, y)$ is the distance between grid cell (i, j) and (x, y). $U_{L_{(i,j)}}$ is the speed of the climatological low-level wind (LLW) at the grid (i, j); this is normalized across all the NC grid cells. Here we consider LLW as the vertical average of winds at levels lower than 850 hPa where short-range transport mostly occurs. Over the mountainous areas with elevation higher than 850 hPa, LLW is averaged within the PBL. $\theta_{(i,j)}(x, y)$ is the angle between the direction of the LLW and the direction from the grid cell (i, j) to (x, y) (referred to as the "LLW angle"). The truncation distance coefficient D_{T0} is set to 200 km. Equation (9) indicates that the influence of emissions at the grid cell (x, y) rapidly decreases with $D_{T_{(i,j)}}(x, y)$. $D_{T_{(i,j)}}(x, y)$ varies with LLW speed and angle at grid cell (i, j). A large LLW speed and a small LLW angle (i.e., (x, y) located downwind of (i, j)) means that emissions at the grid cell (i, j) have a strong impact on (x, y) and a relatively long transport range in that direction. In contrast, small LLW speed implies a minor impact of $E_{(i,j)}$ in all directions.

Third, we rescale the $E_S(x, y)$ over the whole of NC with a scaling factor of 10 to keep the ASI_E dimensionless and on the order of magnitude of one, as was done for ASI_M. Hence the quantity P_E is in the form of:

$$P_E = \frac{E_S - \min(E_S)}{\max(E_S) - \min(E_S)} \times 10, \quad (11)$$

where the "min" and "max" denote the minimum and maximum of E_S over NC, respectively. Equation (7) suggests that P_E is a spatial weighting function, which provides the fixed emission background for ASI_M. It does not vary with time (either interannually or interseasonally) and makes ASI_E more realistic in reflecting the spatial distribution of haze-related meteorology. The temporal variations in ASI_E are not impacted by P_E because of the use of fixed emissions $E_{(i,j)}$ and climatological LLW speeds $U_{L_{(i,j)}}$ for each grid cell. In other words, for a specific grid cell or site in NC, the ASI_E is still a *pure meteorological index* that reflects the variability of local haze-related weather conditions. This notion is analogous to sensitivity studies using fixed emission inventories in chemical transport model simulations (Feng et al., 2016; Mu and Liao, 2014).

The daily ASI_E is calculated using daily reanalysis data (see section 2.2), and the monthly, annual and climatological ASI_E are derived from the mean of daily ASI_E. We perform long-term trend and IAV analyses for the annual and December–January–February (DJF) mean series of ASI_E. The maximum percentage deviation (MxPD) and mean percentage deviation (MnPD) (Feng et al., 2016; Mu and Liao, 2014; Fu and Liao, 2012) are used to represent the relative largest and mean IAV in ASI_E, respectively; these can be written as:

$$MxPD = \frac{\max(ASI_E) - \min(ASI_E)}{\min(ASI_E)} \times 100\%, \quad (12)$$

$$MnPD = \frac{\frac{1}{N}\sum_{i=1}^{N}\left|ASI_{Ei}^{'}\right|}{\overline{ASI_E}} \times 100\%, \quad (13)$$

where $\overline{ASI_E}$ and $ASI_{E_i}^{'}$ denote the long-term mean of ASI_E and its deviation in the ith year. N is the size of the time-series (number of years). MxPD and MnPD denote the quantified variability of haze-related weather conditions in NC. We calculate the ASI_E and apply the trend

and IAV analyses separately at each reanalysis grid cell. Other statistical methods used in this study include correlation and linear regression analysis, which are all statistically tested at 99% confidence. The linear trends are presented as percentages using the 1980 value as the benchmark.

2.2. Meteorology, emissions and $PM_{2.5}$ data

The MERRA-2 (Modern-Era Retrospective Analysis for Research and Applications, version 2, real-time available at https://disc.sci.gsfc.nasa.gov) (Gelaro et al., 2017) daily meteorological data from 1980 to 2018 are used to calculate the daily ASI_E. The horizontal resolution of MERRA-2 is 0.5 ° × 0.625 °. More information on the applicability of MERRA-2 data to air stagnation studies over NC may be found in Feng et al. (2018).

The emission quantities used here for calculating E (Eq. (8)) are from the Multi-resolution Emission Inventory for China (MEIC) provided by Tsinghua University (http://www.meicmodel.org) for the year 2012 on a resolution of 0.25 ° × 0.25 °. The emissions are categorized into five sectors including power, industry, residential, transportation, and agriculture. The MEIC is a bottom-up inventory and provides both gaseous and particle species related to $PM_{2.5}$, including SO_2, NO_x, non-methane volatile organic compounds, NH_3, BC, OC and other $PM_{2.5}$ emissions. Since this study focuses on the temporal variation in ASI, we use the annually averaged MEIC datasets to obtain the fixed $PM_{2.5}$-related emissions. In addition, to match the horizontal resolution of the emission inventory with the meteorological data, we interpolated the emission quantities (in kg km^{-2}) onto the MERRA-2 grid cells using bilinear interpolation, as applied by Matthias et al. (2018) and in the MarcoPolo inventory (http://www.marcopolo.eu/). The close relationship between the $PM_{2.5}$-related emissions E using bilinear and inverse distance weighting methods (with correlation coefficient up to 0.986) indicates that the interpolation methods rarely affect the emission distribution. Fig. 2a shows that E is high over the NC Plain (NCP) and northeastern NC, as observed in previous studies (Zhang et al., 2009, Li et al., 2017a, b). Values of E are relatively high in Beijing, Changchun, Xi'an and in the other capital cities of provinces in NC due to the high level of anthropogenic activity in these urban areas.

To present the effectiveness of ASI_E, we use the observed daily $PM_{2.5}$ concentrations that are averaged from the original MEP/EMC observations (China Ministry of Environmental Protection, Environmental Monitoring Center, real-time accessed at http://113.108.142.147:20035/emcpublish/) from September 2013 to September 2016; approximately 1126 d and 470 sites in total. The spatial distribution of these sites was shown in Fig. 1a in Feng et al. (2018). To match the ASI_E, the observed $PM_{2.5}$ concentrations are interpolated onto MERRA-2 grid cells using inverse distance weighting. To avoid the impact of interpolation error on the estimation, the interpolation is only applied to grid

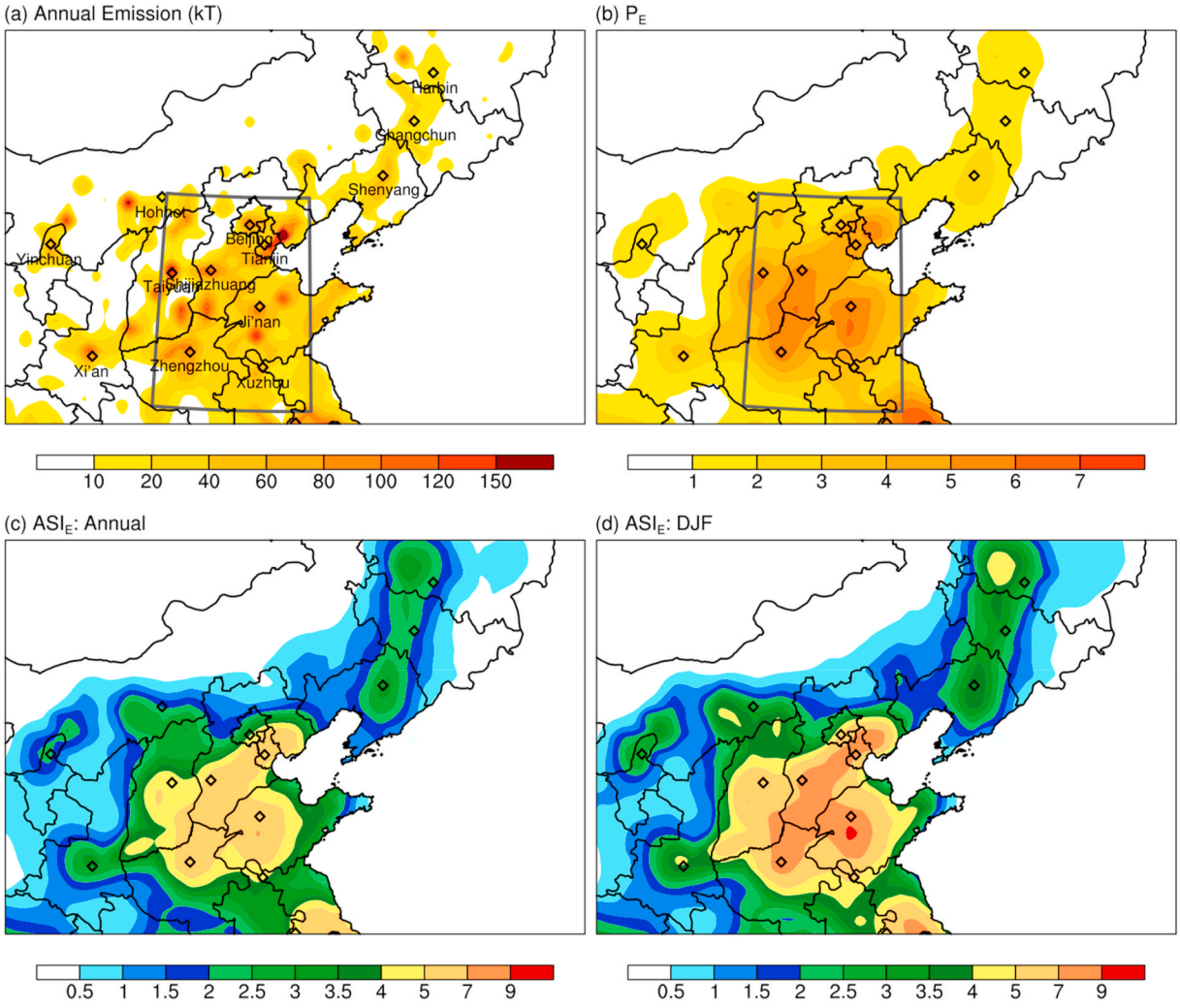

Fig. 2. Geographical distribution of the (a) annual total $PM_{2.5}$-related emissions (kT), (b) emission coefficient (P_E), (c) annually averaged ASI_E and (d) seasonally averaged ASI_E in December–January–February (DJF) in NC from 1980 to 2018. The NCP region and 13 selected cities are indicated by the boxed domain and diamonds in (a), respectively.

cells within 200 km of a site.

3. Results

3.1. ASI_E and its relationship with haze in NC

Fig. 2 shows the geographical distribution of the annual emission E, the emission factor P_E and annually and seasonally averaged ASI_E. The geographical distribution of P_E (Fig. 2b) is similar to that of E (Fig. 2a), with high values over urban areas in NC in both cases. However, the Gaussian smoothing process means that the P_E distribution is smoother than that of E. P_E and E are higher in the NCP than in other areas of NC. The strongest emission belt extends along the line Tianjin–-Shijiazhuang–Zhengzhou, with P_E values greater than 6. High P_E values also cover the areas along Harbin–Changchun–Shenyang, and in the vicinity of other urban areas such as Ji'nan and Xi'an.

Weighted by P_E, the climatological ASI_E also shows a similar distribution (Fig. 2c). The regions with high ASI_E values—around Tianjin–Shijiazhuang–Zhengzhou, Harbin–Changchun–Shenyang and near Ji'nan and Xi'an—also show high P_E values, with the ASI_E value exceeding 5 and 3 in Ji'nan and Xi'an, respectively. These regions with high ASI_E are more sensitive to stagnation weather, which means that under such high emission levels, stagnation conditions will cause severe aerosol pollution. Conversely, in regions with low emissions, such as the mostly rural area of Inner Mongolia and the mountainous area of western NC, even strong air stagnation conditions may not induce haze events (Fig. S1). During DJF, the ASI_E has much higher values over the whole of NC (Fig. 2d), indicating that the stagnation causes worse air quality in winter than in other seasons.

By including the emission information, the ASI_E can reasonably well reflect the spatial distribution of aerosol concentrations, giving a better estimate than ASI_M (Fig. S1). The high (low)-value areas of the climatological ASI_E closely match the areas of high (low) aerosol pollution in NC (Fig. 3a). For example, the "stagnation belts" of Tianjin–-Shijiazhuang–Zhengzhou and Harbin–Changchun–Shenyang also experience severe aerosol pollution. Such spatial agreement can also be

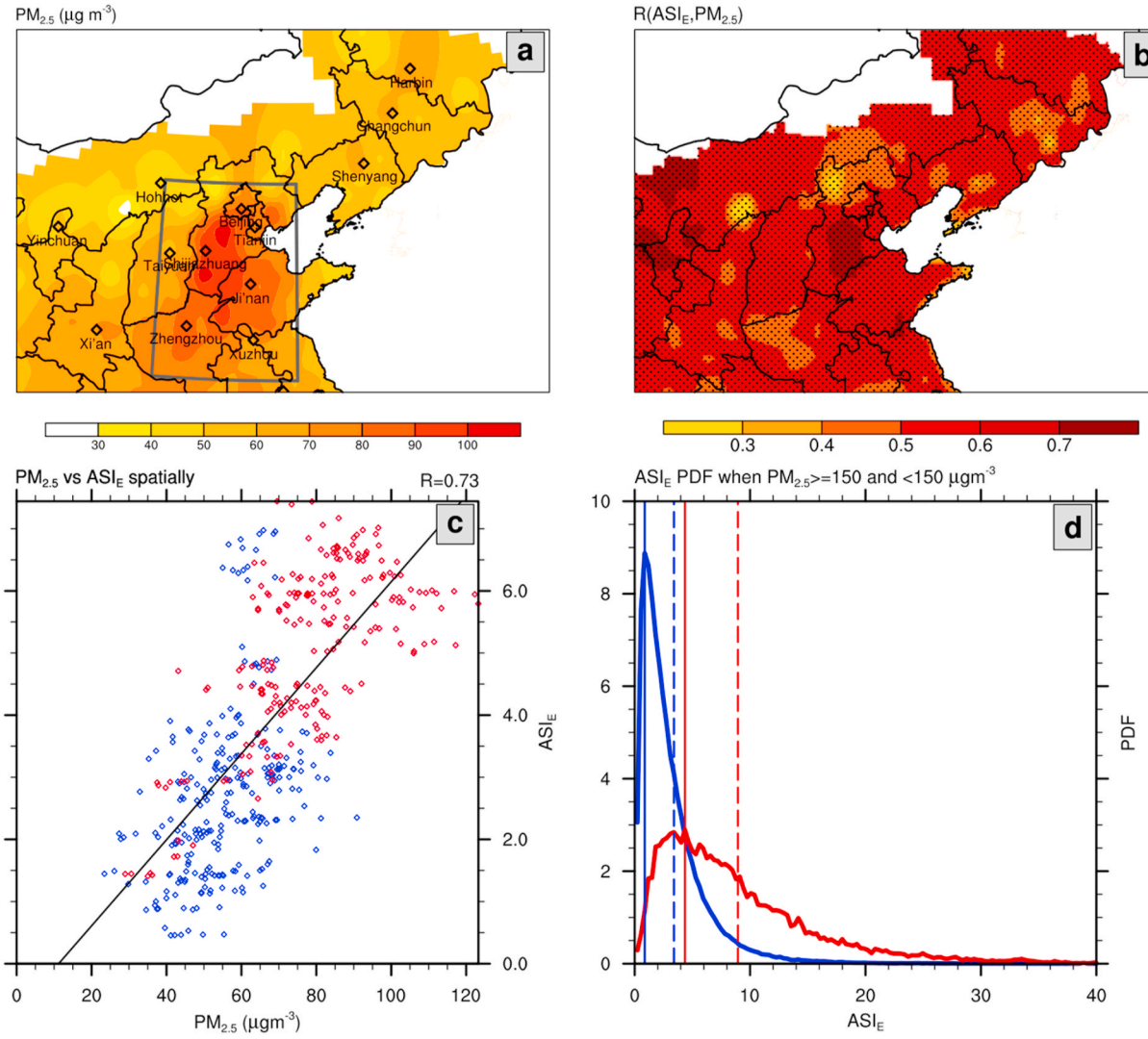

Fig. 3. Geographical distribution of (a) long term-averaged $PM_{2.5}$ concentrations and (b) correlation coefficients between 5-day low-pass filtered time-series of daily ASI_E and $PM_{2.5}$ concentrations from September 01, 2013 to September 30, 2016. The NCP region and selected 13 cities are indicated by the boxed domain and diamonds in (a), respectively. The small black dots in (b) represent the grid cells passing the t-test with a confidence level of 99%. The correlation coefficients in northern Inner Mongolia grid cells, in white, are not involved in the estimation. Panel (c) is a plot between ASI_E and $PM_{2.5}$ over the period from September 01, 2013 to September 30, 2016; the red and blue dots denote the locations in the NCP and other areas of NC, respectively. Panel (d) shows the ASI_E probability distribution function for severe haze days (red thick line; defined as days with $PM_{2.5} > 150$ μg m^{-3}) and other days (blue thick line; defined as days with $PM_{2.5} < 150$ μg m^{-3}) over all observation sites in NC. The red (blue) solid line represents the most likely ASI_E on high- (low-) pollution days. The red (blue) dashed line represents the mean ASI_E on high- (low-) pollution days. (For interpretation of the references to colour in this figure legend, the reader is referred to the Web version of this article.)

shown by the plot between ASI_E and $PM_{2.5}$ concentration (Fig. 3c). Their correlation coefficient (0.73) is much higher than those between $PM_{2.5}$ concentration and surface wind speed, PBLH and ASI_M (Fig. 1). Most sites in the NCP with large ASI_E (red dots) also have correspondingly higher $PM_{2.5}$ concentrations than other areas of NC (blue dots).

The ASI_E can also reflect the temporal variation in aerosol concentrations. Fig. 3b shows correlation coefficients between the daily ASI_E and $PM_{2.5}$ concentrations in every grid cell over NC. Here, the daily time-series are filtered using a 5-day low-pass Lanczos filter (Duchon, 1979). We use a period longer than 5 days because a haze event can last for over 4 days (Wang and Angell, 1999), driven by synoptic-scale activity (Ye et al., 2016). The coefficients are significant at the 99% level according to the *t*-test at all NC grid cells. ASI_E, in particular, performs best in the NCP and western part of NC, with the largest values exceeding 0.7. Since the emission factor is primarily important in spatial terms, such in-situ correlation reflects the impact of the meteorology on aerosol pollution. To further illustrate the relationship between variations in ASI_E and $PM_{2.5}$ concentrations, we examine their 5-day low-pass filtered time-series for 13 selected cities in NC, including Beijing, Tianjin, Shijiazhuang, Xi'an, Zhengzhou, Yinchuan, Ji'nan, Taiyuan, Harbin, Hohhot, Shenyang, Changchun and Xuzhou from September 2013 to September 2016 (Fig. 4). The ASI_E aligns closely with most peaks and troughs of $PM_{2.5}$ concentrations in these cities. In addition, the seasonal variation of $PM_{2.5}$ concentrations can be partly attributed to the more (less) frequent occurrence of stagnant weather in winter (summer) (Qu et al., 2010; Sun et al., 2015; Wang et al., 2015). The high correlation between the ASI_E and $PM_{2.5}$ concentrations in NC is also observed on intra- and inter-seasonal timescales (Fig. S2). According to Eq. (7), these temporal variations in ASI_E reflect the variation in stagnation rather than in emission. Therefore, the close relationship between $PM_{2.5}$ concentration and ASI_E reflects the strong effects of stagnation on $PM_{2.5}$.

To demonstrate the sensitivity of ASI_E to haze occurrence over NC, Fig. 3d shows the probability distributions (PD) of this index for severe haze days ("SHD"; $PM_{2.5}$ concentration $\geq$ 150 μm^{-3}) and other days ("non-SHD") over all days and grid cells (Fig. 3d). The definition of SHD is in accordance with the national air quality standard of China. Both PD curves exhibit a log-normal-like distribution, which is consistent with the typical PD of $PM_{2.5}$ concentrations reported by many previous studies (Šakalys et al., 2004; Ovadnevaitė et al., 2007; Lu, 2002; Feng et al., 2018). However, there are very different values of ASI_E under SHD and non-SHD situations. The SHD curve shifts toward large ASI_E, with the most likely and mean ASI_E values changing from 1.8 to 3.7 for the non-SHD case to 4.5 and 9.0 for SHD, respectively. The distinctive ASI_E values in SHD and non-SHD cases indicate that ASI_E can be used as a reliable indicator of severe haze occurrence in NC.

3.2. Long-term trends in stagnation intensity

Fig. 5a and b presents the time-series and long-term linear trends of the regionally averaged ASI_E for the whole year and DJF during 1980–2018 in NC. There has been a significant amplification of stagnation conditions over the whole of NC in the past 39 years, both annually and during the wintertime. The annual and DJF ASI_E have increased by approximately 4.8% and 4.1% per decade (Table 1), which is equivalent to a total increase of 18.2% and 15.6% since 1980. This increase in ASI_E indicates that air stagnation plays an important role in the long-term increasing frequency of haze events since 1980 (Yang et al., 2018). The bottom panels of Fig. 5 show the regional distribution of the long-term trend of ASI_E. A significant positive trend is observed for the annual ASI_E over a large area of NC, especially in the areas with severe aerosol pollution, such as the NCP, which have regional average trends of approximately 6.5% per decade (Table 1). Of the 13 selected NC cities listed in Table 1, 11 of them (including Tianjin, Shijiazhuang, Ji'nan, Zhengzhou, Xi'an and Xuzhou) exhibit significant positive trends of annual ASI_E. The largest increase is about 9%–10% per decade near Ji'nan. In northeastern NC, the increases in annual ASI_E around Shenyang, Changchun and Harbin are also significant, with a maximum of approximately 7%–8% per decade. In winter, there are eight NC cities showing significant positive trends in ASI_E (Table 1). Most areas of the NCP still show significant positive trends, with the regional average and maximum value in the NCP being 6.0% and about 9%–10%, respectively. In northeastern NC, except for the area near Changchun, the positive trends in annual ASI_E are less significant.

To fully understand the observed significant increase in stagnation intensity, we investigate the long-term variation and trends in the ventilation (inverse of P_V), PBLH (inverse of P_D) and wet deposition factor (P_W in Eq. (1)) for the whole year and DJF during 1980–2018 (Fig. 6). A significant negative trend in ventilation is observed for both the whole year (−1.4% per decade; Table 1) and in wintertime (−1.3% per decade), which is consistent with the declining near-surface wind speed in NC shown by many previous studies (Guo et al., 2011; McVicar et al., 2010; Shi et al., 2019). Over the past 39 years, PBLH showed the same strong decrease (−1.8% and −2% per decade for the whole year and wintertime; Table 1) as ventilation. However, the increase in the wet deposition factor is not significant. Hence, the positive trend for stagnation intensity should be attributed to decreased ventilation and lower PBLH. Table 1 also shows the long-term trends for the ventilation, PBLH and wet deposition factor in NCP and in the 13 selected cities. In NCP, the negative trends for annual ventilation (−1.7% per decade) and PBLH (−3.4% per decade) are larger than those over the whole of NC, indicating that the NCP has worse meteorological conditions than other areas of NC. Therefore, under the highest emission levels in the NCP (Fig. 2), such negative trends would have induced more extreme haze events in recent decades. All 13 cities in NC exhibit negative trends in annual ventilation and PBLH. The strongest negative trend of PBLH is 5.3% per decade, in Ji'nan and Xuzhou, and is likely responsible for the maximum positive trend in ASI_E being near these two cities. Two cities with no significant trend in ASI_E (Shenyang and Hohhot) also show weak negative trends for the ventilation factor and PBLH. The wintertime trends for the three factors are similar but slightly lower than the annual trends in most cities, consistent with the result for the regional mean shown in Fig. 6.

The mechanism for long-term decreased PBLH and ventilation in NC may be worth exploring. The circulation change in the lower troposphere (such as weaker monsoons) and the increase in the drag coefficient, induced by the rapid urbanization over previous decades, may have important implications for decreased wind speed and ventilation (Guo et al., 2011; Wu et al., 2016). In addition, the feedback of aerosol radiative effects that cause a lower PBLH provides another explanation for such negative trends in PBLH (Ding et al., 2016; Li et al., 2017b).

Apart from the overall positive trend, the stagnation intensity also displays some interdecadal variability: the annual ASI_E increased sharply in 1984–1992 and 2000–2005 but fell slowly in 1992–2000 and 2005–2010. The ASI_E achieved a maximum value during 2013–2016 when a series of several haze events occurred, as reported by many previous studies (Quan et al., 2014; Shao et al., 2018a; Ye et al., 2016; Zhang et al., 2014). Note that the ASI_E shows an apparent negative trend during 2013–2018; approximately −5.8% and −3.5% for annual and wintertime means, respectively. This indicates that the recently reported decrease in aerosol concentration in NC since 2013 (http://www.xinhuanet.com/english/2019-01/07/c_137726516.htm) may be partly attributable to the lower stagnation intensity. The interdecadal oscillation during DJF is similar to that of the annual mean: the DJF ASI_E increased steeply during 1984–1992 and 2000–2005 and decreased during 1993–2000 and 2005–2010. The trend and interdecadal oscillation characteristics for ASI_E in DJF resemble the long-term variations in atmospheric visibility and $PM_{2.5}$ concentration, simulated using the CESM (Community Earth System Model) over 1980–2014 (Yang et al., 2018). The decadal variation in ASI_E can be explained by the corresponding variations in ventilation and PBLH (Fig. 6). Prior to 1990, high ventilation and PBLH produced weak stagnation intensity, which

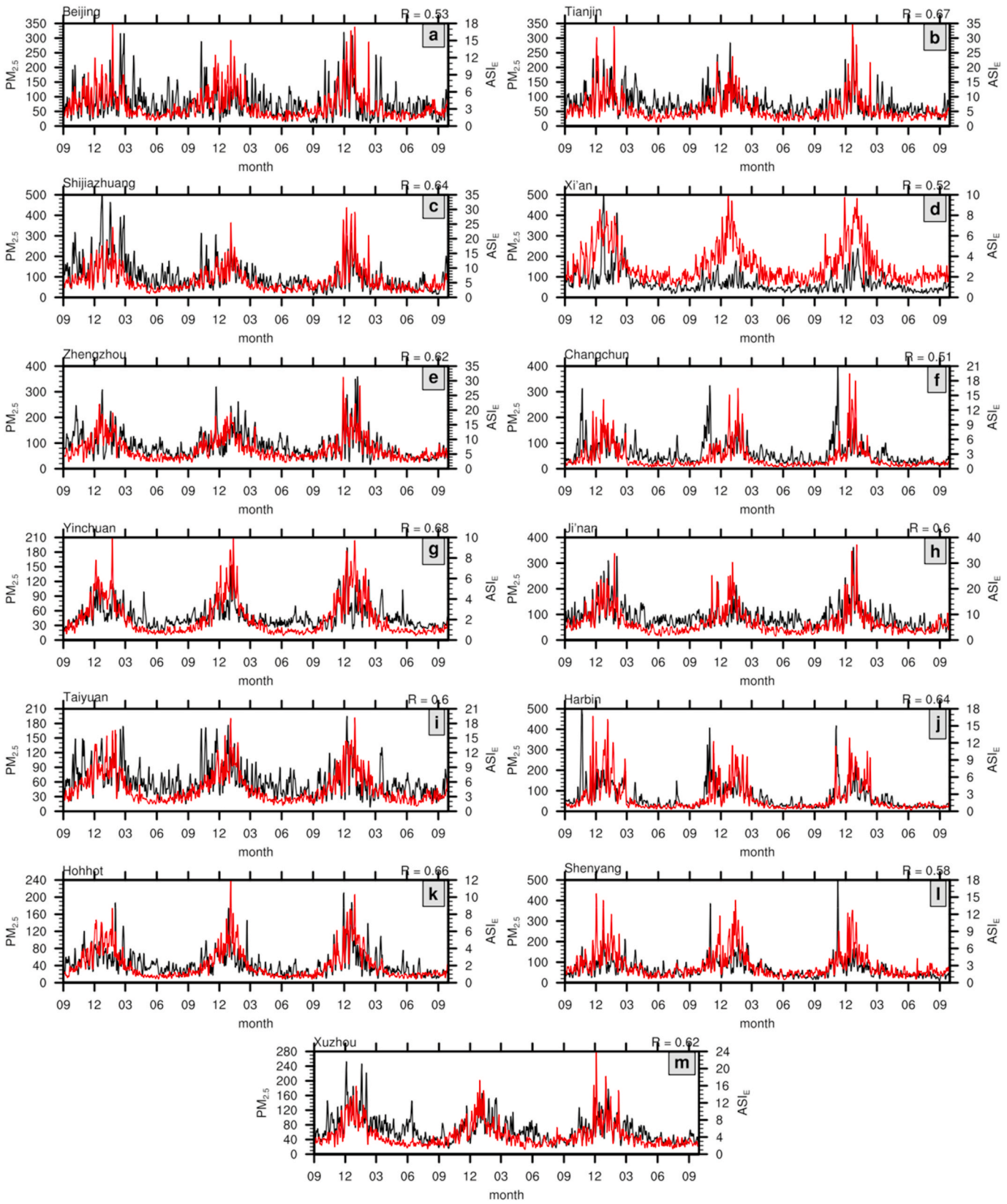

Fig. 4. Low-pass filtered (period ≥ 5 days) time-series of $PM_{2.5}$ concentrations (μg m^{-3}) (black lines) and ASI_E values (red lines) for the 13 selected aerosol-polluted cities shown in Fig. 2a from September 01, 2013 to September 30, 2016. (For interpretation of the references to colour in this figure legend, the reader is referred to the Web version of this article.)

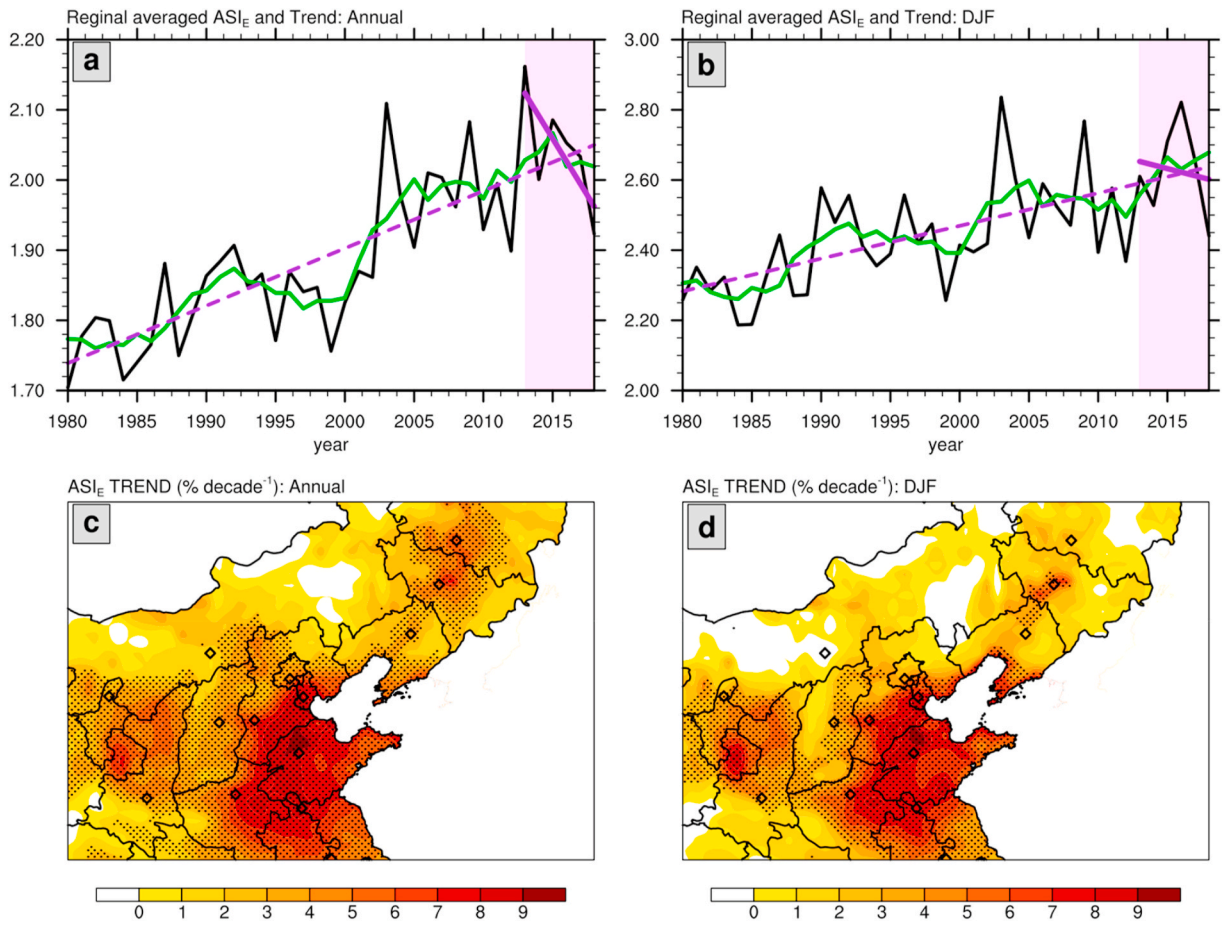

Fig. 5. Time-series of regionally averaged (a) annual and (b) DJF ASI_E during 1980–2018 in NC. The purple dashed line and solid line in (a) and (b) denote the long-term trend in 1980–2018 and in the last 5 yr (i.e., 2013–2018), respectively. The green curves denote a 5-yr running average of the ASI_E series. Plots (c) and (d) present the geographical distributions of long-term annual and DJF ASI_E trends over NC, respectively. Here, the DJF ASI_E refers to the average ASI_E from December of a given year to February of the next year. The dotted areas in (c) and (d) denote where the trend passes the *t*-test with 99% confidence. (For interpretation of the references to colour in this figure legend, the reader is referred to the Web version of this article.)

Table 1
Long-term trends of ASI_E, ventilation, PBLH and wet deposition (P_W) for annual and DJF means over the whole of NC, NCP and 13 selected cities in NC from 1980 to 2018. An asterisk denotes a statistically significant trend at the 99% confidence level using the two-sided *t*-test.

	Trend in annual mean (% decade^{-1})				Trend in DJF (% decade^{-1})			
	ASI_E	Ventilation	PBLH	P_W	ASI_E	Ventilation	PBLH	P_W
NCrowhead	4.8*	−1.4*	−1.8*	0.3	4.1*	−1.3*	−2.0*	0.7
NCP	6.5*	−1.7*	−3.4*	0.4	6.0*	−1.1*	−3.6*	0.5
Beijing	4.1*	−2.4*	−2.5*	0.1	3.4	−1.5	−2.5*	0.6
Tianjin	7.6*	−2.2*	−3.7*	0.2	8.3*	−1.3*	−4.5*	−0.1
Shijiazhuang	6.3*	−2.7	−2.4	0.4	6.8*	−2.6*	−2.5*	−0.1
Xi'an	4.7*	−2.5*	−3.6*	1.0	4.5*	−3.1	−4.7*	1.6
Zhengzhou	7.8*	−0.9	−4.0*	0.5	7.6*	−0.1	−5.2*	1.2
Yinchuan	2.8*	−1.6	−1.9	0.3	2.8*	−2.7	−1.9	1.0
Ji'nan	8.7*	−2.2*	−5.3*	0.9	7.9*	−1.6	−4.4*	0.7
Taiyuan	3.9*	−3.3*	−1.6	0.3	3.4	−2.7	−2.0	0.0
Harbin	6.0*	−1.2	−3.4*	0.0	3.9	−0.8	−1.8	0.5
Hohhot	1.8	−2.2	−1.9	0.6*	−0.7	−1.1*	−1.3	1.4*
Changchun	7.7*	−2.4*	−2.2*	0.2	7.3*	−4.0*	−1.8	1.1
Shenyang	2.9	−1.0	−1.1	0.7	2.7	−0.1	−1.5	1.8
Xuzhou	8.7*	−0.5	−5.3*	0.5	8.2*	−0.5	−5.6*	0.6

suppressed the occurrence of haze events. However, the rapid decrease in ventilation and PBLH during 1999–2013 induced a large surge in haze-related meteorological conditions. In the last 5 years, ventilation and PBLH have begun to increase again and the stagnation intensity and aerosol pollution have subsequently improved. In addition, the above-average wet deposition factor may have an impact on the recent negative trend in ASI_E and haze in NC.

3.3. Interannual variation in stagnation intensity

Fig. 5 exhibits an apparent IAV in regional ASI_E over NC. The MxPD and MnPD of annual (DJF) ASI_E are 26.9% (29.7%) and 5.0% (5.3%),

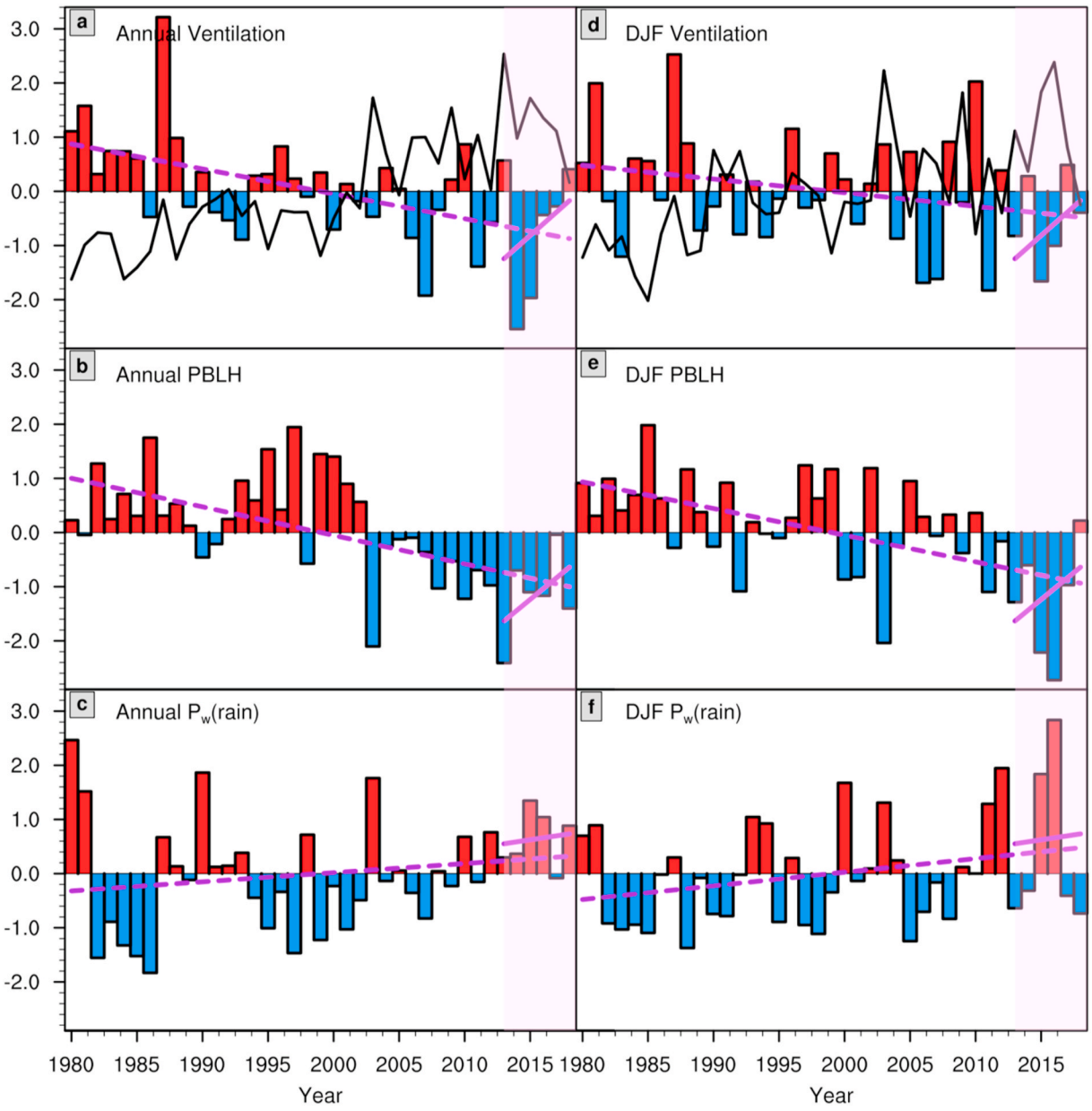

Fig. 6. Standardized series of ventilation, PBLH and wet deposition factor (P_W) for annual (a–c) and DJF (d–f) means. Red and blue bars denote above-and below-average values of series, respectively. The trends in ventilation and PBLH over 1980–2018 and in the last 5 yr (2013–2018) are denoted by purple dashed and solid lines, respectively. The standardized series of annual and DJF ASI_E are also denoted by black curves in (a) and (d) for reference. (For interpretation of the references to colour in this figure legend, the reader is referred to the Web version of this article.)

respectively (Table 2). In other words, variations in the annual-mean and winter-mean haze-related meteorological conditions have a maximum and average magnitude of approximately 30% and 5%, respectively. Since there is a significant trend in the ASI_E series, the MxPD and MnPD of annual (DJF) ASI_E that are recalculated after subtracting linear trends are lower at 18.2% (24.7%) and 2.8% (3.9%), respectively. Comparison between the ASI_E MnPDs calculated with and without the linear trend suggests that most of the IAV of stagnation intensity (especially in winter) is not a result of the long-term trend. Correlation analyses show that the ventilation, PBLH and wet deposition factor are also significantly related to ASI_E. The PBLH has the highest correlation coefficients with ASI_E (−0.73/−0.81 for annual/DJF including the trend and −0.54/−0.66 for annual/DJF excluding the trend), suggesting that the PBLH may have more important effects on the IAV of stagnation intensity in NC than other meteorological variables.

Table 2
Interannual variation of ASI_E in NC, in terms of the MxPD (%) and MnPD (%) for the ASI_E series, with and without long-term trends.

	Annual		DJF	
	with trend	without trend	with trend	without trend
MxPD	26.9	18.2	29.7	24.7
MnPD	5.0	2.8	5.3	3.9

The geographical distribution of MxPD and MnPD of ASI_E indicates there is high IAV in haze-related meteorology in the severely polluted NCP, especially in the southern area near Ji'nan, Zhengzhou and Xuzhou, and in northeastern NC (Fig. 7). The annual MxPD and MnPD in these areas reach 50%–70% and 10%–12%, respectively, which is more than double the regional mean value of NC, suggesting a large IAV in aerosol pollution in these areas. Conversely, haze-related meteorology is more stable in the less-polluted western NC, where the annual MxPD and

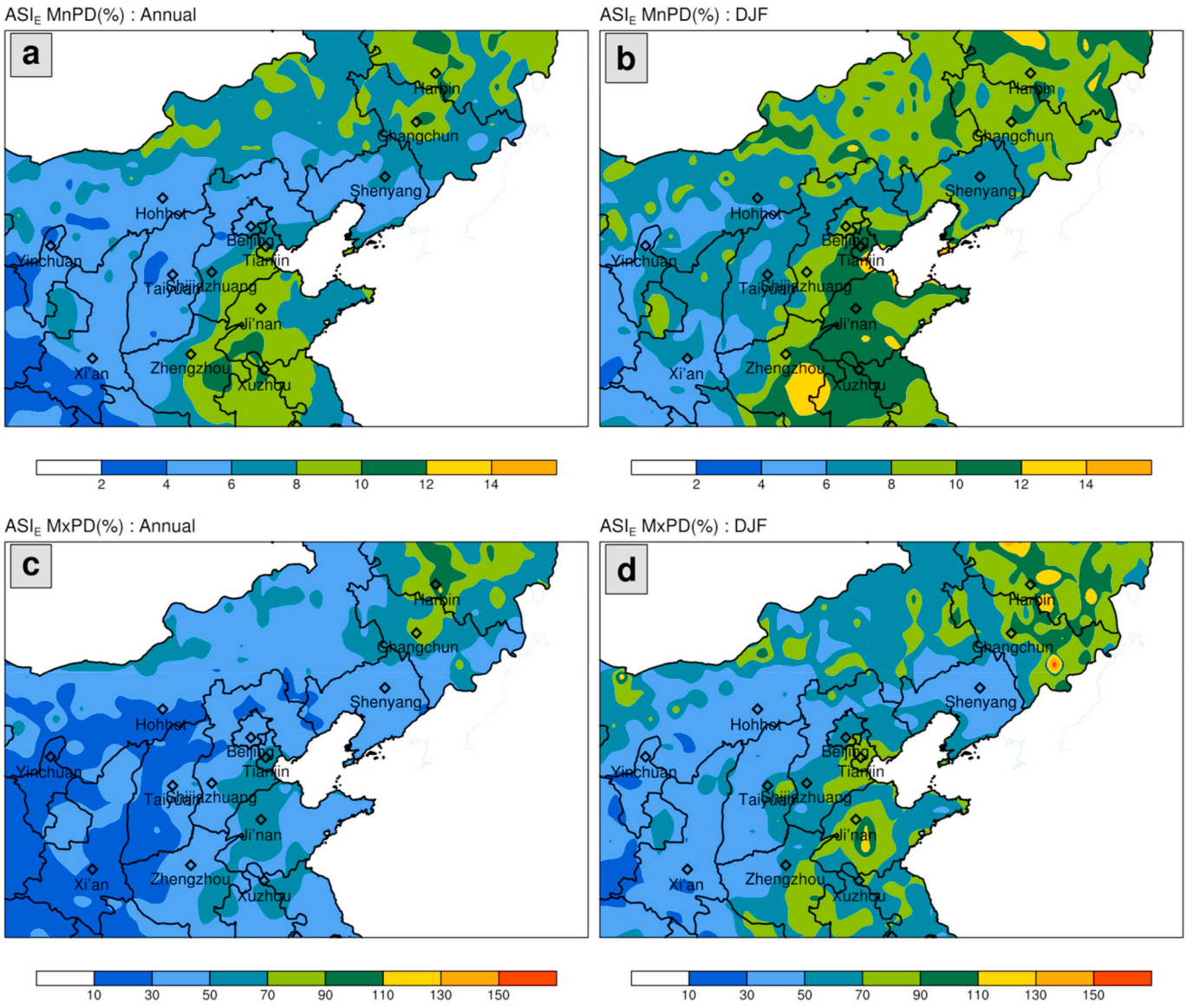

Fig. 7. MnPD (a, b) and MxPD (c, d) for annual ASI_E (a, c) and DJF ASI_E (b, d) over NC during the period 1980–2018. These values are indicative of the IAV of ASI_E.

MnPD are approximately 10%–30% and 2%–6%, respectively. In wintertime, the IAV distribution in ASI_E is generally similar to the annual ASI_E distribution, but with much higher values. The MxPD and MnPD in southern NC exceed 100% and 12% in DJF, respectively, indicating large interannual differences in haze occurrence over the past 39 winters, driven by stagnation intensity. Considering the smaller long-term trend of ASI_E in DJF than for the whole year (Table 1), the IAV of ASI_E excluding the trend in winter should be much stronger than in other seasons.

Under the same emission intensity, the year-to-year changes in ASI_E (Figs. 5 and 7) will cause quite different air quality in different years. The IAV of ASI_E can provide a valuable reference for developing a reasonable and effective emission control strategy. In the areas and years with large increases in ASI_E relative to a specific benchmark year, a moderate emission reduction will not improve air quality. Conversely, a large decrease in ASI_E will cause less haze than the benchmark year even without any emission reduction. Therefore, the year-to-year growth ratio of ASI_E provides some insights into the difficulty of tackling the "clean air challenge" by reducing emissions in NC. Here, we take the year 2013 as a typical example to illustrate this point. Many NC areas reportedly experienced extreme haze events in 2013 (Li et al., 2019; Quan et al., 2014; Shang et al., 2019; Shao et al., 2018a; Tao et al., 2014; Ye et al., 2016; Yin et al., 2017; Zhang et al., 2014). Meanwhile, the stagnation intensity exhibited a large increase in 2013 relative to 2012 (Fig. 5a). Using 2012 as the benchmark year, the ASI_E in 2013 increased in most areas of NC (Fig. 8a), especially in northeastern NC, where the growth ratio reaches ~50%. In NCP, the growth ratio was also high, with the maximum of 30%–40% located north of Ji'nan. The growth ratio was negative in western NC, indicating that haze could be reduced because of the decrease in stagnation in the region, even with no emission reduction.

A recent official report shows a remarkable improvement in China's aerosol pollution in 2018 relative to 2013 (http://www.mee.gov.cn/xxgk2018/xxgk/xxgk15/201906/t20190606_705778.html). Therefore, we also investigate the change of ASI_E in the year 2018 using 2013 as a benchmark year. Most areas of NC have a negative change of ASI_E, including 11 out of all 13 selected cities (Fig. 8b). As the ASI_E does not include the temporal changes in emissions, the officially reported improvement may be partly attributed to the decrease in stagnation intensity from 2013 to 2018. The comparisons between 2013 and 2012 (Fig. 8a) and between 2018 and 2013 (Fig. 8b) suggest that the difficulty rating of the "clean air challenge" should change markedly with the

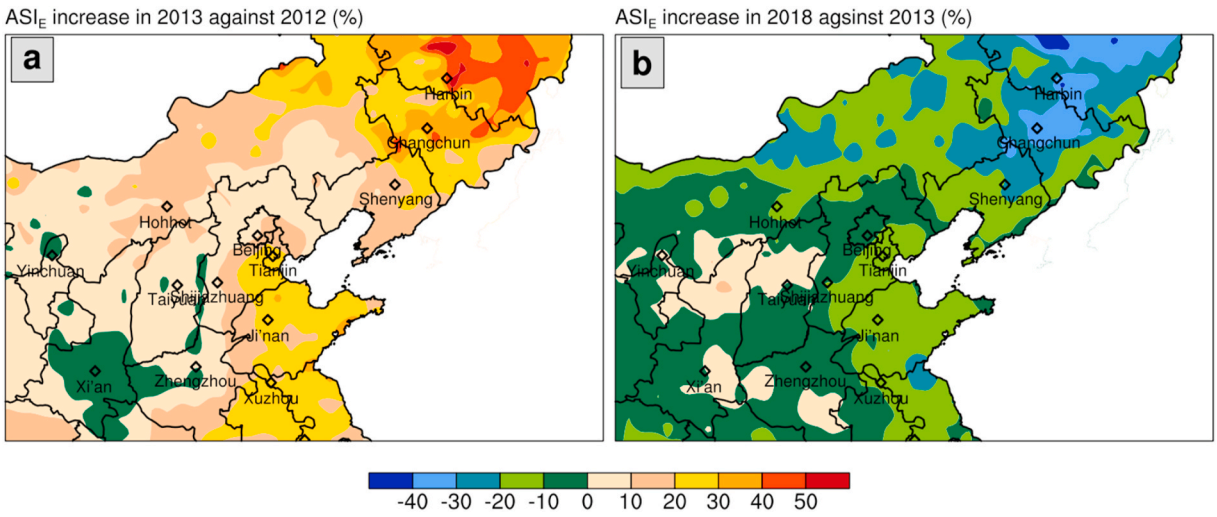

Fig. 8. Growth ratio of ASI_E (%) in (a) 2013 against 2012 and (b) 2018 against 2013.

year, benchmark selection and region. Hence, an emission reduction plan tailored to different years and regions is necessary.

4. Discussion and conclusions

The frequent occurrence of haze events in NC has directed attention to the variations in haze-related meteorology. Most previous studies were mainly based on various statistical indexes or stagnation day frequency indexes. This study investigated the issue using an emission-weighted air stagnation index (ASI_E) that combines a meteorology-based stagnation intensity index, ASI_M, with a spatially (but not temporally) varying emissions factor derived from the MEIC. Including this emission information allows ASI_E to capture the spatial distribution of $PM_{2.5}$ concentrations, improving the results obtained with a pure meteorological index like ASI_M. There are two "stagnation belts" along the lines Tianjin–Shijiazhuang–Zhengzhou and Harbin–Changchun–-Shenyang, which are also severely polluted areas in NC. The ASI_E shows a significant temporal relationship with $PM_{2.5}$ concentrations on different timescales and in all grid cells and several selected big cities in NC. ASI_E is a good indicator for severe haze occurrence due to the strong sensitivity of ASI_E to haze occurrence in NC. Hence, ASI_E could be used to aid climatological analyses of relationships between atmospheric circulation and haze in NC. However, note that the ASI_E cannot reflect variations in the amount of emissions and the corresponding change in aerosol concentrations, because the temporal variation of emissions is not included in the index.

A significant long-term positive trend for stagnation intensity in NC since 1980 is shown, with an 18.2% increase in ASI_E since 1980. The NCP and 11 out of the 13 cities considered exhibited large positive trends of annual ASI_E, with the largest trend of 9%–10% per decade located in the south of the NCP. These long-term trends are mainly caused by significant negative trends in the ventilation and PBLH in NC. ASI_E also shows apparent annual oscillation during the previous 39 years, increasing in 1984–1992 and 1999–2013, but slowly decreasing during 1992–1999 and 2013–2018. The reduced stagnation intensity in the last five years will have contributed to the recent improvement in aerosol concentration in NC. Moreover, the IAV in ASI_E in NC is very strong and is as high as 50%–70% in the severely polluted NCP. Such large year-to-year changes in stagnation intensity may result in quite different air quality under the same emission intensity. Comparison between the growth of ASI_E in 2013 against 2012 and in 2018 against 2013 suggests that the difficulty rating of the "clean air challenge" should change markedly considering the stagnation intensity in each year, benchmark selection and region. Hence, an emission reduction plan tailored to different years and regions is necessary.

This study focuses mainly on the variation and trends in air stagnation intensity over the last 39 years. If the significant positive trend in stagnation intensity continues in the future, haze events in NC will become more severe than current levels. In addition, besides the long-term trend, there is a weak but visible oscillation evident in the 5-yr running average ASI_E (Fig. 5a and b). Peak values occurred around 1990–1992, 2003–2006 and 2013–2016 (i.e., at around 10- to 14-yr intervals). The last peak in 2013–2016 coincides with reports of haze events in the region and the stagnation intensity has been decreasing since that period. If such interdecadal oscillation persists and pushes the ASI_E curve upwards in the future, the long-term positive trend will continue, and haze events will reoccur. Therefore, it is necessary to continually implement a strict emissions policy over the next few years. Future work is welcomed to investigate the mechanisms involved in the long-term oscillation of stagnation intensity and to project future haze-related meteorological conditions in NC.

CRediT authorship contribution statement

Jin Feng: Conceptualization, Methodology, Formal analysis, Investigation, Visualization, Writing - original draft. **Hong Liao:** Writing - review & editing. **Yanjie Li:** Writing - original draft. **Ziyin Zhang:** Resources. **Yingxiao Tang:** Data curation.

Declaration of competing interest

The authors declare that they have no known competing financial interests or personal relationships that could have appeared to influence the work reported in this paper.

Acknowledgements

We thank the anonymous reviewers for their insightful comments and suggestions. This work was supported by the National Natural Science Foundation of China (Grants 41705135, 41705076, and 41790474). MERRA-2 data can be downloaded from https://disc.gsfc.nasa.gov/daac-bin/FTPSubset2.pl. Daily and monthly averaged ASI_M and ASI_E data in NC will be made available on request.

Appendix A. Supplementary data

Supplementary data to this article can be found online at https://doi.org/10.1016/j.atmosenv.2020.117830.

References

Cai, W., Li, K., Liao, H., Wang, H., Wu, L., 2017. Weather conditions conducive to Beijing severe haze more frequent under climate change. Nat. Clim. Change 7, 257–262. https://doi.org/10.1038/nclimate3249.

Chen, H., Wang, H., 2015. Haze days in North China and the associated atmospheric circulations based on daily visibility data from 1960 to 2012. J. Geophys. Res. 120, 5895–5909. https://doi.org/10.1002/2015JD023225.

Chen, S., Guo, J., Song, L., Li, J., Liu, L., Cohen, J.B., 2019. Inter-annual variation of the spring haze pollution over the North China Plain: roles of atmospheric circulation and sea surface temperature. Int. J. Climatol. 39, 783–798. https://doi.org/10.1002/joc.5842.

Ding, A.J., Huang, X., Nie, W., Sun, J.N., Kerminen, V.-M., Petäjä, T., Su, H., Cheng, Y.F., Yang, X.-Q., Wang, M.H., Chi, X.G., Wang, J.P., Virkkula, A., Guo, W.D., Yuan, J., Wang, S.Y., Zhang, R.J., Wu, Y.F., Song, Y., Zhu, T., Zilitinkevich, S., Kulmala, M., Fu, C.B., 2016. Enhanced haze pollution by black carbon in megacities in China. Geophys. Res. Lett. 43, 2873–2879. https://doi.org/10.1002/2016GL067745.

Duchon, C.E., 1979. Lanczos filtering in one and two dimensions. J. Appl. Meteorol. 18, 1016–1022. https://doi.org/10.1175/1520-0450(1979)018<1016:LFIOAT>2.0.CO;2.

Feng, J., Liao, H., Gu, Y., 2016. A comparison of meteorology-driven interannual variations of surface aerosol concentrations in the eastern United States, eastern China, and europe. SOLA 12, 146–152. https://doi.org/10.2151/sola.2016-031.

Feng, J., Quan, J., Liao, H., Li, Y., Zhao, X., 2018. An air stagnation index to qualify extreme haze events in northern China. J. Atmos. Sci. https://doi.org/10.1175/JAS-D-17-0354.1. JAS-D-17-0354.1.

Fu, G.Q., Xu, W.Y., Yang, R.F., Li, J.B., Zhao, C.S., 2014. The distribution and trends of fog and haze in the North China Plain over the past 30 years. Atmos. Chem. Phys. 14, 11949–11958. https://doi.org/10.5194/acp-14-11949-2014.

Fu, Y., Liao, H., 2012. Simulation of the interannual variations of biogenic emissions of volatile organic compounds in China: impacts on tropospheric ozone and secondary organic aerosol. Atmos. Environ. 59, 170–185. https://doi.org/10.1016/j.atmosenv.2012.05.053.

Gelaro, R., McCarty, W., Suárez, M.J., Todling, R., Molod, A., Takacs, L., Randles, C.A., Darmenov, A., Bosilovich, M.G., Reichle, R., Wargan, K., Coy, L., Cullather, R., Draper, C., Akella, S., Buchard, V., Conaty, A., da Silva, A.M., Gu, W., Kim, G.K., Koster, R., Lucchesi, R., Merkova, D., Nielsen, J.E., Partyka, G., Pawson, S., Putman, W., Rienecker, M., Schubert, S.D., Sienkiewicz, M., Zhao, B., 2017. The modern-era retrospective analysis for research and applications, version 2 (MERRA-2). J. Clim. 30, 5419–5454. https://doi.org/10.1175/JCLI-D-16-0758.1.

Guo, H., Xu, M., Hu, Q., 2011. Changes in near-surface wind speed in China: 1969-2005. Int. J. Climatol. 31, 349–358. https://doi.org/10.1002/joc.2091.

Hong, C., Zhang, Q., Zhang, Y., Davis, S.J., Tong, D., Zheng, Y., Liu, Z., Guan, D., He, K., Schellnhuber, H.J., 2019. Impacts of climate change on future air quality and human health in China. Proc. Natl. Acad. Sci. Unit. States Am. 116, 17193–17200. https://doi.org/10.1073/pnas.1812881116.

Horton, D.E., Skinner, C.B., Singh, D., Diffenbaugh, N.S., 2014. Occurrence and persistence of future atmospheric stagnation events. Nat. Clim. Change 4, 1–13. https://doi.org/10.1038/NCLIMATE2272.

Huang, Q., Cai, X., Song, Y., Zhu, T., 2017. Air stagnations for China (1985– 2014): climatological mean features and trends. Atmos. Chem. Phys. 1–23. https://doi.org/10.5194/acp-2016-1072.

Huang, Q., Cai, X., Wang, J., Song, Y., Zhu, T., 2018. Climatological study of the Boundary-layer air Stagnation Index for China and its relationship with air pollution. Atmos. Chem. Phys. 18, 7573–7593. https://doi.org/10.5194/acp-18-7573-2018.

Li, M., Zhang, Q., Kurokawa, J., Woo, J.-H., He, K., Lu, Z., Ohara, T., Song, Y., Streets, D. G., Carmichael, G.R., Cheng, Y., Hong, C., Huo, H., Jiang, X., Kang, S., Liu, F., Su, H., Zheng, B., 2017a. MIX: a mosaic Asian anthropogenic emission inventory under the international collaboration framework of the MICS-Asia and HTAP. Atmos. Chem. Phys. 17, 935–963. https://doi.org/10.5194/acp-17-935-2017.

Li, X., Gao, Z., Li, Y., Gao, C.Y., Ren, J., Zhang, X., 2019. Meteorological conditions for severe foggy haze episodes over north China in 2016–2017 winter. Atmos. Environ. 199, 284–298. https://doi.org/10.1016/j.atmosenv.2018.11.042.

Li, Z., Guo, J., Ding, A., Liao, H., Liu, J., Sun, Y., Wang, T., Xue, H., Zhang, H., Zhu, B., 2017b. Aerosol and boundary-layer interactions and impact on air quality. Natl. Sci. Rev. 4, 810–833. https://doi.org/10.1093/nsr/nwx117.

Lu, H.-C., 2002. The statistical characters of PM10 concentration in Taiwan area. Atmos. Environ. 36, 491–502. https://doi.org/10.1016/S1352-2310(01)00245-X.

Lu, Z., Streets, D.G., de Foy, B., Lamsal, L.N., Duncan, B.N., Xing, J., 2015. Emissions of nitrogen oxides from US urban areas: estimation from Ozone Monitoring Instrument retrievals for 2005–2014. Atmos. Chem. Phys. 15, 10367–10383. https://doi.org/10.5194/acp-15-10367-2015.

Ma, Z., Hu, X., Huang, L., Bi, J., Liu, Y., 2014. Estimating ground-level PM2.5 in China using satellite remote sensing. Environ. Sci. Technol. 48, 7436–7444. https://doi.org/10.1021/es5009399.

Matthias, V., Arndt, J.A., Aulinger, A., Bieser, J., Denier van der Gon, H., Kranenburg, R., Kuenen, J., Neumann, D., Pouliot, G., Quante, M., 2018. Modeling emissions for three-dimensional atmospheric chemistry transport models. J. Air Waste Manag. Assoc. 68, 763–800. https://doi.org/10.1080/10962247.2018.1424057.

McVicar, T.R., Van Niel, T.G., Roderick, M.L., Li, L.T., Mo, X.G., Zimmermann, N.E., Schmatz, D.R., 2010. Observational evidence from two mountainous regions that near-surface wind speeds are declining more rapidly at higher elevations than lower elevations: 1960-2006. Geophys. Res. Lett. 37 https://doi.org/10.1029/2009GL042255 n/a-n/a.

Mu, Q., Liao, H., 2014. Simulation of the interannual variations of aerosols in China: role of variations in meteorological parameters. Atmos. Chem. Phys. 14, 11177–11219. https://doi.org/10.5194/acp-14-9597-2014.

Ovadnevaitė, J., Kvietkus, K., Šakalys, J., 2007. Evaluation of the impact of long-range transport and aerosol concentration temporal variations at the eastern coast of the baltic sea. Environ. Monit. Assess. 132, 365–375. https://doi.org/10.1007/s10661-006-9540-y.

Pei, L., Yan, Z., Sun, Z., Miao, S., Yao, Y., 2018. Increasing persistent haze in Beijing: potential impacts of weakening East Asian winter monsoons associated with northwestern Pacific sea surface temperature trends. Atmos. Chem. Phys. 18, 3173–3183. https://doi.org/10.5194/acp-18-3173-2018.

Qu, W.J., Arimoto, R., Zhang, X.Y., Zhao, C.H., Wang, Y.Q., Sheng, L.F., Fu, G., 2010. Spatial distribution and interannual variation of surface PM 10 concentrations over eighty-six Chinese cities. Atmos. Chem. Phys. 10, 5641–5662. https://doi.org/10.5194/acp-10-5641-2010.

Quan, J., Tie, X., Zhang, Q., Liu, Q., Li, X., Gao, Y., Zhao, D., 2014. Characteristics of heavy aerosol pollution during the 2012–2013 winter in Beijing, China. Atmos. Environ. Times 88, 83–89. https://doi.org/10.1016/j.atmosenv.2014.01.058.

Šakalys, J., Kvietkus, K., Čeburnis, D., Valiulis, D., 2004. The method of determination of heavy metals background concentration in the moss. Environ. Chem. Phys. 26, 109–117.

Shang, H., Letu, H., Pan, X., Wang, Z., Ma, R., Liu, C., Dai, T., Li, S., Chen, L., Chen, C., Hu, Q., 2019. Diurnal haze variations over the North China plain using measurements from Himawari-8/AHI. Atmos. Environ. 210, 100–109. https://doi.org/10.1016/j.atmosenv.2019.04.036.

Shao, P., Tian, H., Sun, Y., Liu, H., Wu, B., Liu, S., Liu, X., Wu, Y., Liang, W., Wang, Y., Gao, J., Xue, Y., Bai, X., Liu, W., Lin, S., Hu, G., 2018a. Characterizing remarkable changes of severe haze events and chemical compositions in multi-size airborne particles (PM1, PM2.5 and PM10) from January 2013 to 2016–2017 winter in Beijing, China. Atmos. Environ. Times 189, 133–144. https://doi.org/10.1016/j.atmosenv.2018.06.038.

Shao, Y., Ulbrich, S., Chen, D., 2018b. Air pumping for alleviation of heavy smog in Beijing. Sci. China Earth Sci. 61, 973–979. https://doi.org/10.1007/s11430-017-9176-8.

Shi, P., Zhang, G., Kong, F., Chen, D., Azorin-Molina, C., Guijarro, J.A., 2019. Variability of winter haze over the Beijing-Tianjin-Hebei region tied to wind speed in the lower troposphere and particulate sources. Atmos. Res. 215, 1–11. https://doi.org/10.1016/j.atmosres.2018.08.013.

Sun, Y.L., Wang, Z.F., Du, W., Zhang, Q., Wang, Q.Q., Fu, P.Q., Pan, X.L., Li, J., Jayne, J., Worsnop, D.R., 2015. Long-term real-time measurements of aerosol particle composition in Beijing, China: seasonal variations, meteorological effects, and source analysis. Atmos. Chem. Phys. 15, 10149–10165. https://doi.org/10.5194/acp-15-10149-2015.

Tao, M., Chen, L., Xiong, X., Zhang, M., Ma, P., Tao, J., Wang, Z., 2014. Formation process of the widespread extreme haze pollution over northern China in January 2013: implications for regional air quality and climate. Atmos. Environ. 98, 417–425. https://doi.org/10.1016/j.atmosenv.2014.09.026.

Wang, J.X.L., Angell, J.K., 1999. Air Stagnation Climatology for the United States (1948-1998).

Wang, X., Dickinson, R.R.E., Su, L., Zhou, C., Wang, K., 2018. PM 2.5 pollution in China and how it has been exacerbated by terrain and meteorological conditions. Bull. Am. Meteorol. Soc. 99, 105–120. https://doi.org/10.1175/BAMS-D-16-0301.1.

Wang, X., Wang, K., Su, L., 2016. Contribution of atmospheric diffusion conditions to the recent improvement in air quality in China. Sci. Rep. 6, 1–11. https://doi.org/10.1038/srep36404.

Wang, Y.Q., Zhang, X.Y., Sun, J.Y., Zhang, X.C., Che, H.Z., Li, Y., 2015. Spatial and temporal variations of the concentrations of PM_{10}, $PM_{2.5}$ and PM_1 in China. Atmos. Chem. Phys. 15, 13585–13598. https://doi.org/10.5194/acp-15-13585-2015.

Wu, P., Ding, Y.H., Liu, Y.J., Li, X.C., 2016. Influence of the East Asian winter monsoon and atmospheric humidity on the wintertime haze frequency over central-eastern China. Acta Meteorol. Sin. 74, 352–366.

Xiao, D., Li, Y., Fan, S., Zhang, R., Sun, J., Wang, Y., 2014. Plausible influence of Atlantic Ocean SST anomalies on winter haze in China. Theor. Appl. Climatol. 249–257. https://doi.org/10.1007/s00704-014-1297-6.

Xin, J., Gong, C., Liu, Z., Cong, Z., Gao, W., Song, T., Pan, Y., Sun, Y., Ji, D., Wang, L., Tang, G., Wang, Y., 2016. The observation-based relationships between PM 2.5 and AOD over China. J. Geophys. Res. Atmos. 121 (10) https://doi.org/10.1002/2015JD024655, 701-10,716.

Yang, Y., Wang, H., Smith, S.J., Zhang, R., Lou, S., Qian, Y., Ma, P.-L., Rasch, P.J., 2018. Recent intensification of winter haze in China linked to foreign emissions and meteorology. Sci. Rep. 8, 2107. https://doi.org/10.1038/s41598-018-20437-7.

Ye, X., Song, Y., Cai, X., Zhang, H., 2016. Study on the synoptic flow patterns and boundary layer process of the severe haze events over the North China Plain in January 2013. Atmos. Environ. 124, 129–145. https://doi.org/10.1016/j.atmosenv.2015.06.011.

Yin, Z., Wang, H., 2016. The relationship between the subtropical western pacific SST and haze over north-central north China plain. Int. J. Climatol. 36, 3479–3491. https://doi.org/10.1002/joc.4570.

Yin, Z., Wang, H., Chen, H., 2017. Understanding severe winter haze events in the North China Plain in 2014: roles of climate anomalies. Atmos. Chem. Phys. 17, 1641–1651. https://doi.org/10.5194/acp-17-1641-2017.

Zhang, Q., Streets, D.G., Carmichael, G.R., He, K.B., Huo, H., Kannari, A., Klimont, Z., Park, I.S., Reddy, S., Fu, J.S., Chen, D., Duan, L., Lei, Y., Wang, L.T., Yao, Z.L., 2009. Asian emissions in 2006 for the NASA INTEX-B mission. Atmos. Chem. Phys. 9, 5131–5153. https://doi.org/10.5194/acp-9-5131-2009.

Zhang, RenHe, Li, Q., Zhang, RuoNan, 2014. Meteorological conditions for the persistent severe fog and haze event over eastern China in January 2013. Sci. China Earth Sci. 57, 26–35. https://doi.org/10.1007/s11430-013-4774-3.

Zhao, S., Li, J., Sun, C., 2016. Decadal variability in the occurrence of wintertime haze in central eastern China tied to the Pacific Decadal Oscillation. Sci. Rep. 6, 27424. https://doi.org/10.1038/srep27424.

Zhu, J., Liao, H., Li, J., 2012. Increases in aerosol concentrations over eastern China due to the decadal-scale weakening of the East Asian summer monsoon. Geophys. Res. Lett. 39, L09809. https://doi.org/10.1029/2012GL051428.